

1 **Complement 3a Receptor 1 on Macrophages and Kupffer cells is not required for the**  
2 **Pathogenesis of Metabolic Dysfunction-Associated Steatotic Liver Disease**

3  
4 Edwin A. Homan<sup>1</sup>, Ankit Gilani<sup>1</sup>, Alfonso Rubio-Navarro<sup>1</sup>, Maya Johnson<sup>1</sup>, Eric Cortada<sup>1</sup>, Renan  
5 Pereira de Lima<sup>1</sup>, Lisa Stoll<sup>1</sup>, James C. Lo<sup>1\*</sup>.

6  
7 **Affiliations:**

8 <sup>1</sup> Division of Cardiology, Department of Medicine, Cardiovascular Research Institute, Weill  
9 Center for Metabolic Health, Weill Cornell Medicine, New York, New York, 10021

10 \*Corresponding author. Email: [jlo@med.cornell.edu](mailto:jlo@med.cornell.edu).

11

12

13

14 **Abstract**

15 Together with obesity and type 2 diabetes, metabolic dysfunction-associated steatotic liver  
16 disease (MASLD) is a growing global epidemic. Activation of the complement system and  
17 infiltration of macrophages has been linked to progression of metabolic liver disease. The role of  
18 complement receptors in macrophage activation and recruitment in MASLD remains poorly  
19 understood. In human and mouse, *C3AR1* in the liver is expressed primarily in Kupffer cells, but  
20 is downregulated in humans with MASLD compared to obese controls. To test the role of  
21 complement 3a receptor (C3aR1) on macrophages and liver resident macrophages in MASLD,  
22 we generated mice deficient in C3aR1 on all macrophages (C3aR1-M $\phi$ KO) or specifically in  
23 liver Kupffer cells (C3aR1-KpKO) and subjected them to a model of metabolic steatotic liver  
24 disease. We show that macrophages account for the vast majority of *C3ar1* expression in the  
25 liver. Overall, C3aR1-M $\phi$ KO and C3aR1-KpKO mice have similar body weight gain without  
26 significant alterations in glucose homeostasis, hepatic steatosis and fibrosis, compared to  
27 controls on a MASLD-inducing diet. This study demonstrates that C3aR1 deletion in  
28 macrophages or Kupffer cells, the predominant liver cell type expressing *C3aR1*, has no  
29 significant effect on liver steatosis, inflammation or fibrosis in a dietary MASLD model.

30

31 **Keywords:** obesity, hepatic steatosis, steatohepatitis, C3aR1, macrophage, Kupffer cell

32

## 33 Introduction

34 Obesity and related metabolic diseases such as type 2 diabetes (T2D) and metabolic  
35 dysfunction-associated steatotic liver disease (MASLD) remain a worldwide epidemic with  
36 increasing prevalence<sup>1,2</sup>. MASLD describes the constellation of hepatic lipid deposition,  
37 inflammation, and fibrosis associated with obesity and T2D that ultimately leads to MASH  
38 cirrhosis, which has become the leading cause of liver transplantation in the United States<sup>3-6</sup>.  
39 Notably, MASLD is increasingly recognized as an important risk-enhancing factor for  
40 atherosclerotic cardiovascular disease<sup>7,8</sup>.

41 Liver macrophages help to maintain hepatic homeostasis and consist of embryo-derived  
42 resident macrophages called Kupffer cells, which self-renew and do not migrate, or peripheral  
43 monocyte-derived macrophages, which infiltrate into liver tissue upon metabolic or toxic liver  
44 injury and under certain circumstances can take on Kupffer cell-like identity<sup>9-13</sup>. In obesity, bone  
45 marrow-derived myeloid cells migrate to the steatotic liver, and pro-inflammatory recruited  
46 macrophages are postulated to drive the progression of MASLD to MASH<sup>14</sup>. Spatial  
47 proteogenomics reveals a population of lipid-associated macrophages near bile canaliculi that is  
48 induced by local lipid exposure and drives fibrosis in steatotic regions of murine and human  
49 liver<sup>15</sup>. In addition, deep transcriptomic profiling in human MASLD has identified candidate gene  
50 signatures for steatohepatitis and fibrosis with possible therapeutic implications<sup>16</sup>.

51 Activation of the body's complement system leads to increased cell lysis, phagocytosis,  
52 and inflammation<sup>17</sup>, and it is increasingly recognized as an important contributor to regulation of  
53 metabolic disorders such as T2D and MASLD<sup>18,19</sup>. In human liver biopsies, higher lobular  
54 inflammation scores correlate with activation of the complement alternative pathway<sup>20</sup>, which  
55 can signal *via* the C3a receptor 1 (C3aR1), a G<sub>i</sub>-coupled G protein-coupled receptor<sup>21</sup>. The  
56 complement 3 polypeptide (C3) is cleaved by C3 convertase to the activated fragment, C3a,  
57 which then binds C3aR1<sup>22</sup>. Complement factor D (CFD), also known as the adipokine adipsin, is  
58 the rate-limiting step in the alternative pathway of complement activation<sup>23,24</sup>.

59           Several studies have reported opposing roles of adiponectin and C3aR1 on hepatic steatosis  
60 in diet-induced obesity<sup>25-27</sup>. Our lab has found that adiponectin/CFD is critical for maintaining  
61 pancreatic beta cell mass and function<sup>28,29</sup>. Murine obese and diabetic models such as *db/db*  
62 mice and high fat diet (HFD) feeding result in very low circulating adiponectin<sup>23</sup>. Replenishing adiponectin  
63 in *db/db* mice raises levels of C3a and insulin, lowers blood glucose levels, and inhibits hepatic  
64 gluconeogenesis<sup>28</sup>. However, whole-body deletion of C3aR1 decreases macrophage infiltration  
65 and activation in adipose tissue, protects from HFD-induced obesity and glucose intolerance,  
66 and decreases hepatic steatosis and inflammation<sup>30</sup>. In a model of fibrosing steatohepatitis,  
67 bone marrow-derived macrophages were found to activate hepatic stellate cells, which was  
68 blunted in whole-body C3aR1 KO mice<sup>31</sup>.

69           In the present study we aim to explore the macrophage-specific effect of complement  
70 receptor signaling in MASLD pathogenesis. To determine the consequences of macrophage and  
71 Kupffer cell ablation of C3aR1, we use a murine dietary model of MALFD/MASH, the Gubra  
72 Amylin Nash (GAN) diet, which has macronutrient similarities to the Western diet and produces  
73 similar histologic and transcriptomic changes to human MASLD/MASH<sup>32-34</sup>.

74

## 75 **Results**

76 *C3AR1 is expressed in human and mouse liver, primarily in Kupffer cells.*

77           In the scRNA-Seq database, Human Protein Atlas, *C3AR1* is broadly expressed  
78 throughout the body, with increased abundance in tissues rich in immunologic cell types, such  
79 as bone marrow and appendix (Fig. 1A)<sup>35</sup>. In a single-cell transcriptomic database of healthy  
80 human liver, *C3AR1* expression predominates in the macrophage and Kupffer cell population,  
81 with minimal-to-undetectable *C3AR1* expression in hepatocytes or hepatic stellate cells by  
82 scRNA-Seq (Fig. 1B)<sup>36</sup>. In the mouse liver scRNA-Seq database, Tabula Muris, *C3ar1* is  
83 similarly expressed primarily in Kupffer cells (Fig. S1)<sup>37</sup>.

84

85 *Hepatic CFD and C3AR1 are downregulated in human MASLD/MASH.*

86 We also examined data from Suppli and coworkers, who performed bulk transcriptomic  
87 analysis of human liver samples from an age-matched cohort of healthy controls and obese  
88 controls without MASLD, as well as MASLD and MASH patients without cirrhosis<sup>38</sup>. Both *CFD*  
89 *and C3AR1* were unchanged in obese subjects without MASLD compared to healthy controls,  
90 but both *CFD* and *C3AR1* were significantly downregulated in liver biopsies from both MASLD  
91 and MASH patients compared to both healthy controls and obese subjects without MASLD (Fig.  
92 1C). Interestingly, both *CFD* and *C3AR1* levels were slightly higher in MASH individuals  
93 compared to those with MASLD only.

94

95 *Murine MASH model recapitulates key features of human MASH*

96 At 5 weeks of age, we subjected *C3ar1* flox/flox control mice to standard regular diet  
97 (RD) or GAN diet<sup>32,33</sup>. After 28 weeks of GAN diet, male mice gained body weight compared to  
98 RD (Fig. 1D), primarily as fat mass (Fig. S2-3), but weight gain in female GAN-fed mice was  
99 attenuated. Histologic signs of MASLD were present in GAN-fed mice (Fig. 1E), most notably  
100 hepatic steatosis and hepatocyte ballooning (Fig. 1F), and liver fibrosis measured by collagen  
101 deposition nearly doubled with GAN compared to RD (Fig. 1G). Both hepatic *C3ar1* and *Cfd*  
102 gene expression were robustly increased on GAN compared to RD, as were markers of  
103 macrophage infiltration, hepatic inflammation, and fibrosis, including collagen gene expression,  
104 indicating progression to fibrotic MASH (Fig. 1H).

105

106 *Macrophage-specific C3aR1 deletion does not alter glucose homeostasis.*

107 Owing to the differential regulation of the *C3AR1* gene in MASLD between mice and  
108 humans, we generated transgenic mice with macrophage-specific deletion of C3aR1 (*C3aR1*-  
109 *MφKO*) to target both liver resident macrophages and recruited monocytes. Successful deletion  
110 of *C3ar1* in macrophages from the *C3aR1*-*MφKO* mouse was confirmed by quantitative RT-

111 PCR of isolated peritoneal macrophages that were F4/80+ and CD68+ by fluorescence-  
112 activated cell sorting (Fig. 2A). In liver tissue, *C3ar1* expression was reduced by ~88% in both  
113 male and female C3aR1-M $\phi$ KO (Fig. 2B). These results indicate that macrophages account for  
114 the vast majority of *C3ar1* expression in the liver.

115 When placed on GAN diet, there was no significant difference in weight gain between  
116 control and C3aR1-M $\phi$ KO mice (Fig. 2C). There was similarly no difference in percent lean or  
117 fat mass between these mice (Fig. 2D). Glucose tolerance tests performed in fasted mice after  
118 27 weeks GAN diet found no significant differences between control and C3aR1-M $\phi$ KO mice  
119 (Fig. 2E). There was also no difference in insulin sensitivity as measured by insulin tolerance  
120 tests in male mice (Fig. S4). Insulin resistance as measured by comparing the ratio of fasting  
121 glucose level to fasting insulin level (HOMA-IR) was also unchanged between controls and  
122 C3aR1-M $\phi$ KO mice (Fig. S5). Circulating serum ALT levels were unchanged in male control and  
123 C3aR1-M $\phi$ KO mice on GAN diet (Fig. S6).

124

125 *Macrophage-specific C3aR1 deletion does not significantly impact hepatic steatosis or fibrosis.*

126 Liver samples collected after 28-30 weeks of GAN or regular diet did not show significant  
127 differences in liver mass between control and C3aR1-M $\phi$ KO mice (Fig. 2F). Male mice on GAN  
128 diet developed similar qualitative appearance on histology (Fig. 2G), and slide image analysis  
129 showed similar proportions of lipid droplet area and collagen area (Figs. 2H, 2I). This indicates  
130 that there were no significant differences in steatosis or fibrosis between GAN-fed control and  
131 C3aR1-M $\phi$ KO male mice. While *C3ar1* expression was markedly reduced in the C3aR1-M $\phi$ KO  
132 liver tissue (Fig. 2B), there were no detectable gene expression changes in markers of fibrosis,  
133 inflammation, or lipid handling (Fig. 2J). Similarly, in female mice there were also no significant  
134 differences between control and C3aR1-M $\phi$ KO mouse liver in a subset of key gene markers of  
135 fibrosis or inflammation (Fig. S7).

136

137 *Kupffer cell-specific C3aR1 deletion does not alter weight gain or glucose homeostasis.*

138 To explore whether there may be competing effects between recruited monocytes and  
139 liver resident macrophages (Kupffer cells), we next generated Kupffer cell-specific C3aR1  
140 knockout mice (C3aR1-KpKO) and fed them GAN diet. Body weight gain was similar between  
141 genotypes for both male and female mice (Fig. 3A), and there was no difference in body  
142 composition between control and C3aR1-KpKO mice on GAN diet (Fig. 3B). There was similarly  
143 no significant difference in glucose homeostasis between the genotypes during a glucose  
144 tolerance test (Fig. 3C).

145

146 *Kupffer cell-specific C3aR1 deletion does not significantly impact hepatic steatosis or fibrosis.*

147 Liver mass was not significantly different between control and C3aR1-KpKO mice on  
148 GAN diet (Fig. 3D). Liver sections appeared qualitatively similar by histology stained with  
149 Masson's trichrome (Fig. 3E). There were similar levels of hepatic steatosis in these mice as  
150 measured by percent lipid droplet area (Fig. 3F). When measured by collagen proportional area,  
151 there was no significant differences in liver fibrosis between C3aR1-KpKO and control mice  
152 (Fig. 3G). While *C3ar1* expression was reduced by 73% in liver tissue of C3aR1-KpKO mice,  
153 there were no significant differences in expression of inflammatory, fibrotic, or lipid handling  
154 gene markers (Fig. 3H). *C3ar1* expression similarly decreased by ~90% in liver tissue of female  
155 C3aR1-KpKO mice fed regular diet compared to control mice (Fig. S8). These data also indicate  
156 that Kupffer cells account for ~80% of hepatic *C3ar1* gene expression in our mouse model of  
157 MASLD/MASH.

158

## 159 **Discussion**

160 Overall, we found that macrophage or Kupffer cell expression of *C3ar1* does not impact  
161 body weight gain or histologic/transcriptomic features of MASLD/MASH in a murine dietary

162 model. Deletion of C3aR1 in the macrophage population throughout the body, or specifically in  
163 Kupffer cells, did not affect weight gain, glucose homeostasis, or extent of hepatic  
164 steatosis/fibrosis.

165 Our findings in macrophage-specific C3aR1 KO mice contrast with prior observations in  
166 whole-body C3aR1 KO mice<sup>30</sup>, which are protected from diet-induced obesity, have improved  
167 glucose tolerance, and exhibit decreased hepatic steatosis. In both our macrophage- and  
168 Kupffer cell-specific C3aR1 KO mice, which had similar degrees of obesity compared to  
169 controls, there was no detectable effect on liver steatosis or fibrosis despite the near abrogation  
170 of *C3ar1* expression. This raises the possibility that the lower levels of hepatic steatosis and  
171 insulin resistance previously observed in the whole body C3aR1 KO mice may be secondary to  
172 protection from obesity. Protection from diet-induced obesity in whole-body C3aR1 KO mice  
173 may be mediated by a non-macrophage cell type, since our macrophage-specific C3aR1 KO  
174 mice were not afforded this protection. The *C3ar1*-expressing cell types that promote obesity  
175 and MASLD remains to be determined.

176 Our laboratory recently reported sex-dependent regulation of thermogenic adipose  
177 tissue mediated by adipocyte-derived C3aR1<sup>39</sup>. However, no such sexual dimorphism was  
178 observed in hepatic expression of key MASH genes in response to GAN diet in our  
179 macrophage- or Kupffer cell-specific C3aR1-deficient mice. Other work has suggested possible  
180 compensatory effects from its sister anaphylatoxin receptor C5aR1, with increased cold-induced  
181 adipocyte browning and attenuated diet-induced obesity seen in C3aR1/C5aR1 double KO  
182 mice<sup>40</sup>.

183 The strengths of our study include careful metabolic and transcriptomic phenotyping of  
184 cell type-specific transgenic mice. Some limitations were our use of a single MASLD dietary  
185 model and our focus on the C3aR1 pathway. While the GAN diet recapitulates many features of  
186 human MASH due to its similarity to Western diet<sup>34</sup>, relatively low levels of fibrosis were seen in  
187 our study, potentially related to initiating the diet at young age; more rapid fibrosis induction has



188 been seen when GAN diet is initiated at older ages<sup>41</sup>. Lastly, while *C3AR1/C3ar1* expression is  
189 very low in non-macrophage cells (Fig. B, S1), C3aR1 signaling on other hepatic cell types not  
190 explored in this study, such as hepatic stellate cells, could mediate the observed effect in the  
191 whole-body C3aR1 KO mouse.

192 Deletion of C3aR1 in macrophages generally, or in liver resident macrophages  
193 specifically, had no major effect on systemic glucose homeostasis and hepatic steatosis,  
194 inflammation, and fibrosis in this murine dietary model of MASLD/MASH. The complement  
195 system is a complex entity directing an important part of the body's inflammatory and tissue  
196 repair response in MASLD. Further work is needed to elucidate the mechanisms of the role of  
197 C3aR1 in the pathogenesis of MASH and cirrhosis.

198

## 199 **Materials and Methods**

### 200 *Animals*

201 *C3ar1 flox/flox* mice were on the C57BL/6J background as described<sup>42</sup>. Homozygous  
202 LysM-Cre mice on the C57BL/6J background were purchased from Jackson Laboratories  
203 (Strain #004781). *C3ar1 flox/flox* homozygous mice were used in the experiments as controls  
204 from the same backcross generation<sup>39</sup>. All mice were maintained in plastic cages under a  
205 12h/12h light/dark cycle at constant temperature (22°C) with free access to water and food.  
206 Mice were fed regular diet containing 4.5%kcal fat PicoLab Rodent diet 20 (LabDiet) or GAN  
207 diet containing 40%kcal HFD (mostly palm oil) with 20% fructose and 2% cholesterol  
208 (D09100310, Research Diets) for 28-30 weeks. Fat mass and lean mass were determined via  
209 noninvasive 3-in-1 body composition analyzer (EchoMRI). Mice were humanely euthanized with  
210 CO<sub>2</sub> inhalation followed by exsanguination by cardiac puncture.

211

### 212 *Blood chemistry and serum insulin analysis*

213 Mice were fasted overnight (14-16 hours) for glucose tolerance tests and injected  
214 intraperitoneally with syringe-filtered D-glucose solution (2g/kg). For insulin tolerance test, mice  
215 were fasted for 6 hours and injected with 0.5 mIU/kg insulin. Blood glucose levels were assayed  
216 by commercial glucometer (OneTouch) by tail vein blood samples. Plasma insulin levels were  
217 measured from mice fasted for 6 hours. Tail vein blood was collected into lithium heparin-coated  
218 tubes, centrifuged at 2000xg at 4°C, and plasma insulin levels were determined by ELISA using  
219 a standard curve (Merckodia). Serum alanine aminotransferase levels were measured in serum  
220 from blood collected via cardiac puncture using a commercially available colorimetric assay  
221 (TR71121, ThermoFisher Scientific).

222

#### 223 *Peritoneal macrophage isolation and flow cytometry*

224 Peritoneal macrophages were isolated from as previously described<sup>43</sup>. Briefly, mice  
225 were euthanized then immediately injected intraperitoneally with 10 mL phosphate-buffered  
226 saline (PBS, pH 7.4) at room temperature. After a 3-5 minute incubation period, peritoneal fluid  
227 was removed with sterile needle and syringe and placed on ice. After centrifugation at 300xg,  
228 the pellet was resuspended in PBS containing 2% fetal bovine serum and 0.1% sodium azide.  
229 Cells were stained with phycoerythrin-conjugated anti-F4/80 (clone BM8, cat. #123110) and  
230 fluorescein isothiocyanate-conjugated anti-CD11b (clone M1/70, cat. #101206) fluorescent  
231 antibodies (Biolegend). Stained cells were loaded on MA900 fluorescence-activated cell sorter  
232 (Sony), and dual-positive F480+/CD11b+ cells were sorted for subsequent RNA extraction.

233

#### 234 *Histological studies*

235 A mid-distal portion of the left liver lobe was fixed with 10% buffered formalin and  
236 transferred to 70% ethanol. Samples were embedded in paraffin, sectioned at ~5µm thickness,  
237 and stained with Masson's trichrome. Slides were imaged using Zeiss Axioscan7 at 20x  
238 magnification. Histologic analyses were performed using ImageJ software (version 1.53t). Lipid

239 droplet area was quantified by subtracting non-droplet area in the green channel from total  
240 section area of 2-3 independent sections. Collagen proportionate area was quantified by  
241 measuring total area in the red channel after reducing intensity threshold to 60-70.

242

#### 243 *RNA extraction and real-time quantitative PCR analysis*

244 Total RNA from liver tissue lysates was extracted using Trizol reagent (Invitrogen)  
245 followed by RNAeasy Mini kit (Qiagen) as per manufacturer's protocol. RNA was reverse-  
246 transcribed using the High Capacity cDNA RT kit (Thermo). Quantitative PCR was performed  
247 using SYBR Green Master Mix (Quanta) and specific gene primers on QuantStudio6 Flex Real-  
248 Time PCR Systems (Thermo Fisher Scientific) using the delta-delta Ct method. Expression  
249 levels were normalized to Ribosomal protein S18 (*Rps18*). Primer sequences are listed in  
250 Supplementary Table A.

251

#### 252 *Statistical analyses*

253 All statistical analyses were performed using GraphPad Prism10. Unpaired two-tailed  
254 Student's *t* test with Welch correction for most analyses, with Holm-Šídák correction for multiple  
255 comparisons where applicable, and  $p < 0.05$  was considered statistically significant.

256

#### 257 **Funding**

258 E.A.H. was supported by NIH T32 5T32HL160520-02. A.G. was supported by was  
259 supported by ADA 9-22-PDFPM-01. R.P.L was supported by AHA 23DIVSUP1074485. L.S. was  
260 supported by AHA 908952 and an Ehrenkranz Young Scientist Award. J.C.L. was supported by  
261 NIH R01 DK121140, R01 DK121844, and R01 DK132879. The views expressed in this  
262 manuscript are those of the authors and do not necessarily represent the official views of the  
263 American Diabetes Association, the American Heart Association, the National Institute of  
264 Diabetes and Digestive and Kidney Diseases, or the National Institutes of Health.

265

266 **Acknowledgments**

267 We would like to thank Dr. Baran Ersoy, Dr. Robert Schwartz, and Dr. Saloni Sinha for their  
268 technical advice and assistance.

269

270 **Declaration of Competing Interest**

271 None

272

273 **Data Availability**

274 Data will be made available upon reasonable request.

275

276 **Figure Legends**

277

278 **Figure 1. C3AR1 is found in macrophages, is modulated by MASLD/MASH in humans,**  
279 **and is induced by a murine dietary model of MASH.**

280 A) Relative *C3AR1* human tissue expression level by tissue, derived from deep sequencing  
281 of the mRNA combined dataset (HPA and GTEx) in the Human Protein Atlas, shown as  
282 normalized transcripts per million (nTPM). Liver is highlighted in purple and immunologic  
283 tissues are highlighted in red.

284 B) Single-cell RNA sequencing distribution of *C3AR1* expression in human liver (tSNE, t-  
285 distributed Stochastic Neighbor Embedding).

286 C) Analysis of *CFD* and *C3AR1* expression from liver biopsy samples in patients with  
287 MASH, MASLD, obesity without MASLD, and age-matched healthy controls (n = 12-16  
288 per group, Welch *t* test with Holm-Šídák correction for multiple comparisons).

289 D) Weight curve in male and female flox/flox control mice placed on GAN high-fat diet  
290 compared to regular diet (RD) controls (males, n = 7; females, n = 6).

291 E) Representative liver section staining by Masson's Trichrome in male control mice on RD  
292 or GAN diet for 28 weeks (scale bar = 100  $\mu$ m).

293 F) Lipid droplet area quantification in liver sections from male control mice, excluding  
294 vessel lumens (RD, n = 3; GAN, n = 7).

295 G) Collagen area quantification in liver sections of male control mice (RD, n = 3; GAN, n =  
296 7).

297 H) Gene expression of key macrophage or fibrosis genes in male control mice on GAN or  
298 RD (n = 6 per group).

299 Unpaired two-tailed Student's *t* test (Except 1C as above). Annotations: \*, p < 0.05; \*\*, p < 0.01;

300 \*\*\*, p < 0.001

301 **Figure 2. C3aR1 deletion in all macrophages does not affect weight gain, glucose**  
302 **homeostasis, liver steatosis or fibrosis.**

- 303 A) Expression of *C3ar1* in isolated peritoneal F4/80+/CD68+ cells from flox/flox control mice  
304 (n = 6) or C3aR1-M $\phi$ KO male mice (n = 3).
- 305 B) Expression of *C3ar1* in whole liver from control or C3aR1-M $\phi$ KO mice (n = 11-12 per  
306 male group, n = 13-14 per female group).
- 307 C) Body mass curve of control or C3aR1-M $\phi$ KO mice on GAN high-fat diet starting at 5  
308 weeks of age (n = 11-12 per male group, n = 14 per female group).
- 309 D) Body composition analysis by EchoMRI in control or C3aR1-M $\phi$ KO mice after 30 weeks  
310 GAN diet (n = 6-9 per male group, n = 9-13 per female group).
- 311 E) Glucose tolerance test in control or C3aR1-M $\phi$ KO mice with 14h fast after 28 weeks  
312 GAN diet (n = 6-9 per male group, n = 9-14 per female group).
- 313 F) Liver mass in control or C3aR1-M $\phi$ KO male mice at time of euthanasia after 30 weeks  
314 GAN diet (n = 6-9 per male group, n = 9-14 per female group).
- 315 G) Representative liver section staining by Masson's Trichrome in male control or C3aR1-  
316 M $\phi$ KO mice (scale bar = 100  $\mu$ m).
- 317 H) Lipid droplet area in liver sections from male control or C3aR1-M $\phi$ KO mice, excluding  
318 vessel lumens (n = 6-7 per group).
- 319 I) Collagen area in liver sections from male control or C3aR1-M $\phi$ KO mice (n = 6-7 per  
320 group)
- 321 J) Relative fold expression of key gene markers for fibrosis, inflammation, and liver  
322 metabolism in whole liver from male control or C3aR1-M $\phi$ KO mice mice after 30 weeks  
323 GAN diet (n = 11-12 per group).

324 Unpaired two-tailed Student's *t* test: Student's *t* test: \*, p < 0.05.

325

326 **Figure 3. C3aR1 deletion in Kupffer cells does not affect weight gain, glucose**  
327 **homeostasis, liver steatosis or fibrosis.**

- 328 A) Body mass curve on GAN diet in flox/flox control or C3aR1-KpKO mice beginning at 5  
329 weeks of age (n = 8-10 per group).
- 330 B) Body composition analysis by EchoMRI in control or C3aR1-KpKO mice after 28 weeks  
331 GAN diet (n = 8-10).
- 332 C) Glucose tolerance test in control or C3aR1-KpKO mice with 14h fast after 26 weeks  
333 GAN diet (n = 8-10).
- 334 D) Liver mass in control or C3aR1-KpKO male mice at time of euthanasia after 30 weeks  
335 GAN diet (n = 8-10).
- 336 E) Representative liver section staining by Masson's Trichrome in control or C3aR1-KpKO  
337 male mice (scale bar = 100  $\mu$ m).
- 338 F) Lipid droplet area quantified on liver sections of control or C3aR1-KpKO male mice ,  
339 excluding vessel lumens (n = 8-9).
- 340 G) Collagen area quantified on whole liver section of control or C3aR1-KpKO male mice (n=  
341 8-9).
- 342 H) Relative gene expression in male control or C3aR1-KpKO mice after 30 weeks GAN diet  
343 (n = 5-6).

344 Unpaired two-tailed Student's *t* test: \*\*, p < 0.01.

345

346 **Supplementary figures.**

347 S1) Single cell RNA sequencing analysis of *C3ar1* expression in mouse liver tissue (see  
348 text).

349 S2) Percent lean and fat mass of flox/flox control mice after 20 weeks of GAN or RD diet (n =  
350 6-7 per group).

351 S3) Absolute lean and fat mass of flox/flox control mice after 20 weeks of GAN or RD diet (n  
352 = 6-7 per group).

353 S4) Insulin tolerance test in control or C3aR1-M $\phi$ KO male mice with 14h fast after 29 weeks  
354 GAN diet (n = 6-9 per group).

355 S5) HOMA-IR measurement of insulin resistance in control or C3aR1-M $\phi$ KO mice with 6h  
356 fast after 27 weeks GAN diet (n = 6-9 per male group, n = 9-13 per female group).

357 S6) Serum alanine aminotransferase levels in control or C3aR1-M $\phi$ KO male mice after 30  
358 weeks GAN diet (n = 4 per group).

359 S7) Relative gene expression in control or C3aR1-M $\phi$ KO female mice after 30 weeks GAN  
360 diet (n = 13-14 per group).

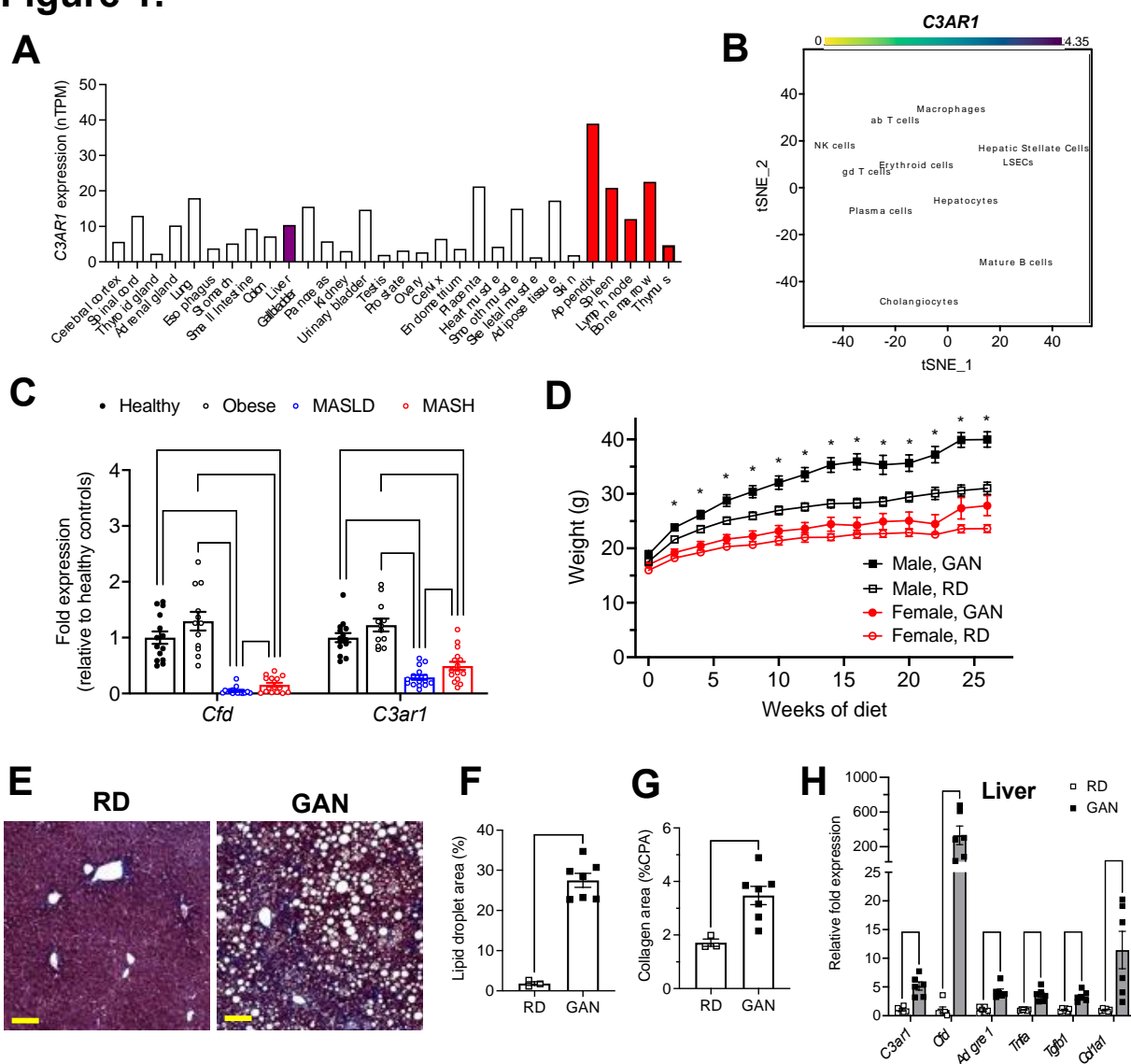
361 S8) Relative *C3ar1* expression in control or C3aR1-KpKO female mice after 30 weeks RD  
362 diet (n = 2-3 per group).

363 Unpaired two-tailed Student's *t* test: \*\*, p < 0.01; \*\*\*, p < 0.001.

364



## Figure 1.



365

**Figure 1. C3AR1 is found in macrophages, is modulated by MASLD/MASH in humans, and is induced by a murine dietary model of MASH.**

- A) Relative *C3AR1* human tissue expression level by tissue, derived from deep sequencing of the mRNA combined dataset (HPA and GTEx) in the Human Protein Atlas, shown as normalized transcripts per million (nTPM). Liver is highlighted in purple and immunologic tissues are highlighted in red.
- B) Single-cell RNA sequencing distribution of *C3AR1* expression in human liver (tSNE, t-distributed Stochastic Neighbor Embedding).
- C) Analysis of *CFD* and *C3AR1* expression from liver biopsy samples in patients with MASH, MASLD, obesity without MASLD, and age-matched healthy controls (n = 12-16 per group, Welch *t* test with Holm-Šidák correction for multiple comparisons).
- D) Weight curve in male and female flox/flox control mice placed on GAN high-fat diet compared to regular diet (RD) controls (males, n = 7; females, n = 6).
- E) Representative liver section staining by Masson's Trichrome in male control mice on RD or GAN diet for 28 weeks (scale bar = 100  $\mu$ m).
- F) Lipid droplet area quantification in liver sections from male control mice, excluding vessel lumens (RD, n = 3; GAN, n = 7).
- G) Collagen area quantification in liver sections of male control mice (RD, n = 3; GAN, n = 7).
- H) Gene expression of key macrophage or fibrosis genes in male control mice on GAN or RD (n = 6 per group). Unpaired two-tailed Student's *t* test (Except 1C as above). Annotations: \*, p < 0.05; \*\*, p < 0.01; \*\*\*, p < 0.001.

366  
367

## Figure 2.

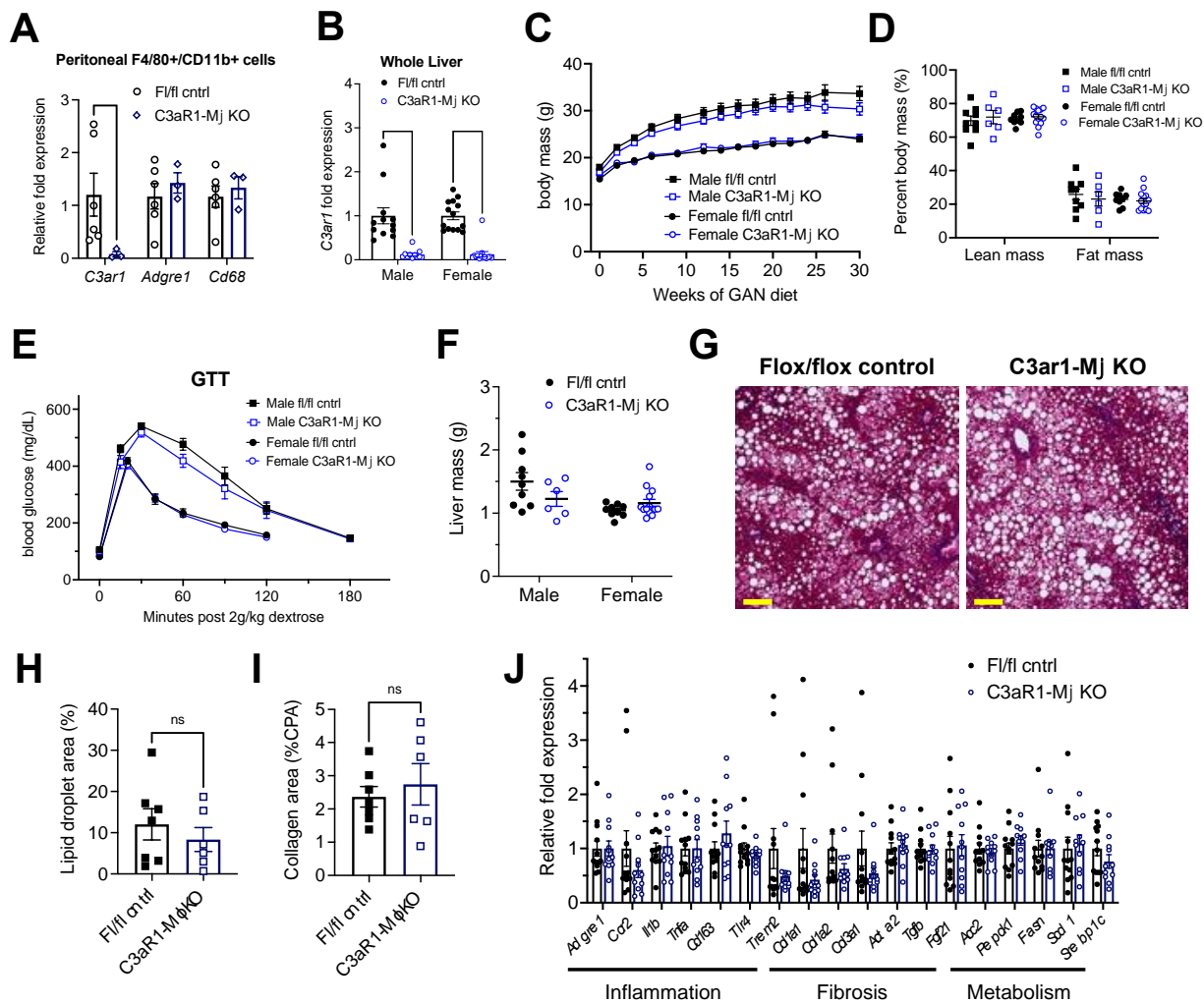


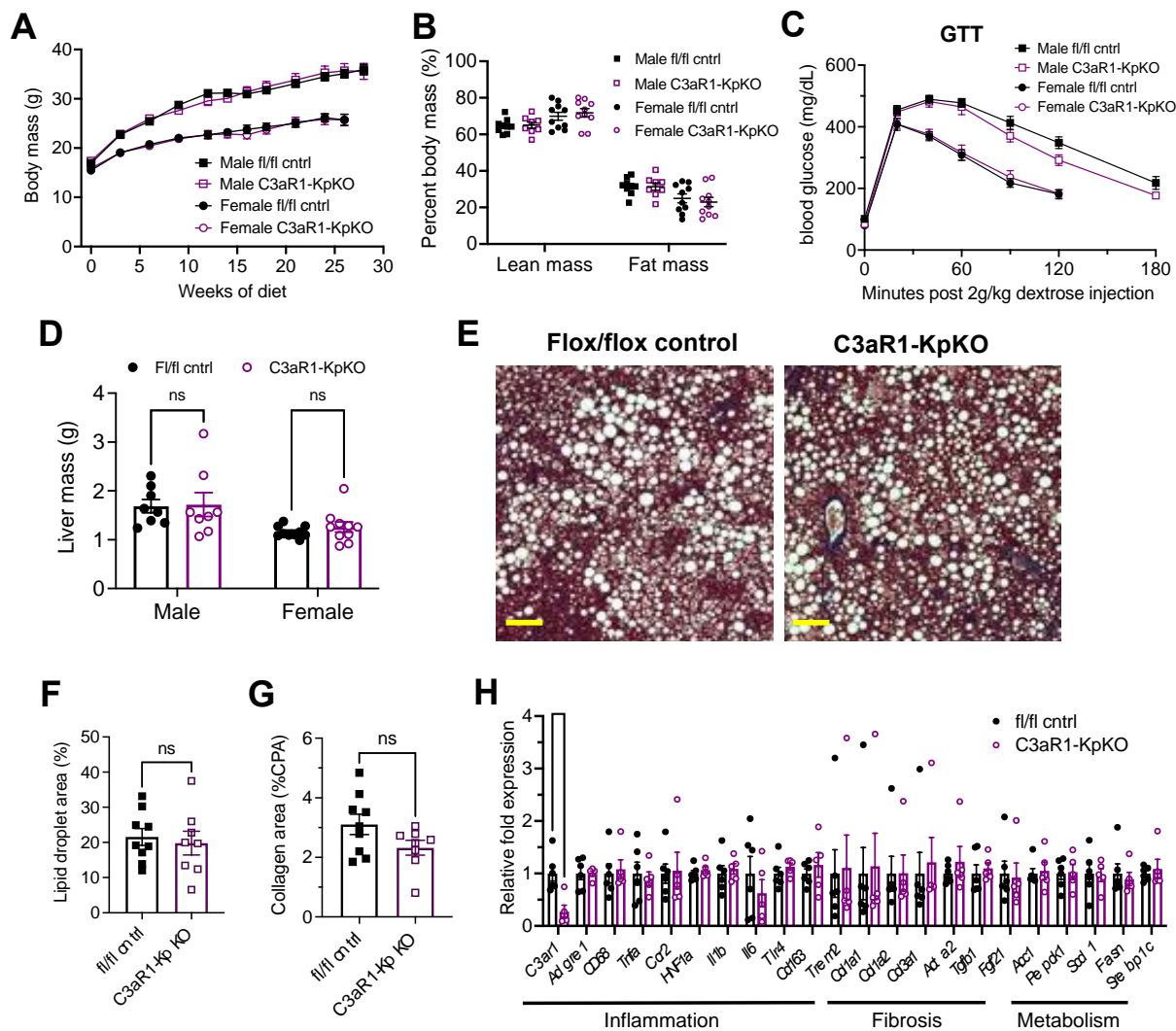
**Figure 2. C3aR1 deletion in all macrophages does not affect weight gain, glucose homeostasis, liver steatosis or fibrosis.**

- A) Expression of *C3ar1* in isolated peritoneal F4/80+/CD11b+ cells from floxed control mice (n = 6) or C3aR1-Mj KO male mice (n = 3).
- B) Expression of *C3ar1* in whole liver from control or C3aR1-Mj KO mice (n = 11-12 per male group, n = 13-14 per female group).
- C) Body mass curve of control or C3aR1-Mj KO mice on GAN high-fat diet starting at 5 weeks of age (n = 11-12 per male group, n = 14 per female group).
- D) Body composition analysis by EchoMRI in control or C3aR1-Mj KO mice after 30 weeks GAN diet (n = 6-9 per male group, n = 9-13 per female group).
- E) Glucose tolerance test in control or C3aR1-Mj KO mice with 14h fast after 28 weeks GAN diet (n = 6-9 per male group, n = 9-14 per female group).
- F) Liver mass in control or C3aR1-Mj KO male mice at time of euthanasia after 30 weeks GAN diet (n = 6-9 per male group, n = 9-14 per female group).
- G) Representative liver section staining by Masson's Trichrome in male control or C3aR1-Mj KO mice (scale bar = 100  $\mu$ m).
- H) Lipid droplet area in liver sections from male control or C3aR1-Mj KO mice, excluding vessel lumens (n = 6-7 per group).
- I) Collagen area in liver sections from male control or C3aR1-Mj KO mice (n = 6-7 per group).
- J) Relative fold expression of key gene markers for fibrosis, inflammation, and liver metabolism in whole liver from male control or C3aR1-Mj KO mice after 30 weeks GAN diet (n = 11-12 per group).
- Unpaired two-tailed Student's *t* test: Student's *t* test: \*, *p* < 0.05.

368  
369

370

## Figure 3.



371  
372

**Figure 3. C3aR1 deletion in Kupffer cells does not affect weight gain, glucose homeostasis, liver steatosis or fibrosis.**

A) Body mass on GAN diet in flox/flox control or C3aR1-KpKO mice beginning at 5 weeks of age (n = 8-10 per group).

B) Body composition analysis by EchoMRI in control or C3aR1-KpKO mice after 28 weeks GAN diet (n = 8-10).

C) Glucose tolerance test in control or C3aR1-KpKO mice with 14h fast after 26 weeks GAN diet (n = 8-10).

D) Liver mass in control or C3aR1-KpKO male mice at time of euthanasia after 28 weeks GAN diet (n = 8-10).

E) Representative liver section staining by Masson's Trichrome in control or C3aR1-KpKO male mice (scale bar = 100  $\mu$ m).

F) Lipid droplet area quantified on liver sections of control or C3aR1-KpKO male mice, excluding vessel lumens (n = 8-9).

G) Collagen area quantified on whole liver section of control or C3aR1-KpKO male mice (n = 8-9).

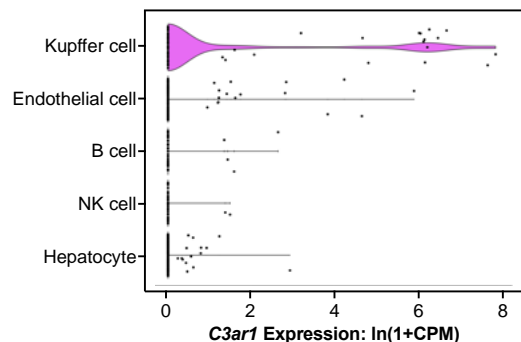
H) Relative gene expression in control or C3aR1-KpKO male mice after 30 weeks GAN diet (n = 5-6).

Unpaired two-tailed Student's *t* test: \*\*, *p* < 0.01.

373

## Supplementary Figures.

**S1**



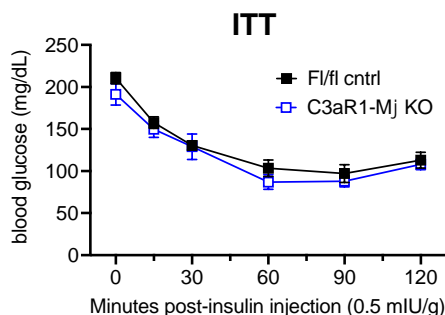
**S2**



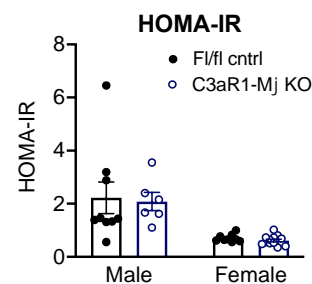
**S3**



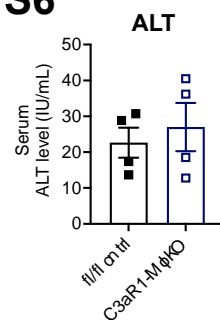
**S4**



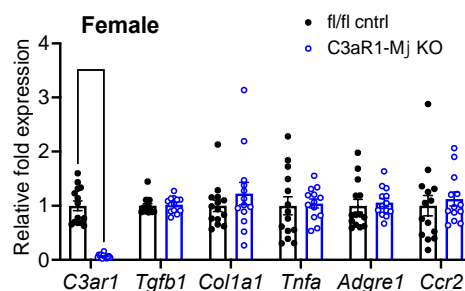
**S5**



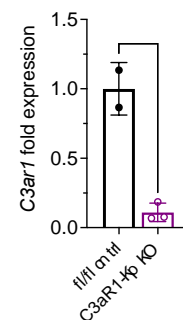
**S6**



**S7**



**S8**



374  
375

### Supplementary figures.

- S1) Single cell RNA sequencing analysis of *C3ar1* expression in mouse liver tissue (see text).  
 S2) Percent lean and fat mass of flox/flox control mice after 20 weeks of GAN or RD diet (n = 6-7 per group).  
 S3) Absolute lean and fat mass of flox/flox control mice after 20 weeks of GAN or RD diet (n = 6-7 per group).  
 S4) Insulin tolerance test in control or C3aR1-Mj KO male mice with 14h fast after 29 weeks GAN diet (n = 6-9 per group).  
 S5) HOMA-IR measurement of insulin resistance in control or C3aR1-Mj KO mice with 6h fast after 27 weeks GAN diet (n = 6-9 per male group, n = 9-13 per female group).  
 S6) Serum alanine aminotransferase levels in control or C3aR1-Mj KO male mice after 30 weeks GAN diet (n = 4 per group).  
 S7) Relative gene expression in control or C3aR1-Mj KO female mice after 30 weeks GAN diet (n = 13-14 per group).  
 S8) Relative *C3ar1* expression in control or C3aR1-KpKO female mice after 30 weeks RD diet (n = 2-3 per group).  
 Unpaired two-tailed Student's *t* test: \*\*, p < 0.01; \*\*\*, p < 0.001.

376

377 **Supplementary Table S1.**

<b><i>Mus musculus</i> gene name</b>	<b>Forward qPCR primer</b>	<b>Reverse qPCR primer</b>
Acc2	GCCTCCACTCACATTGGTTT	ATTGAAGAAAGCTGGGCTGA
Acta2	GGCTCTGGGCTCTGTAAGG	CTCTTGCTCTGGGCTTCATC
Adgre1	TGCATCTAGCAATGGACAGC	GCCTTCTGGATCCATTTGAA
C3ar1	TGACAGGTCAGCTCCTTCCT	CATTAGGAGGCTTTCCACCA
Ccr2	ATCCACGGCATACTATCAACATC	CAAGGCTCACCATCATCGTAG
Cd163	TCCACACGTCCAGAACAGTC	CCTTGAAACAGAGACAGGC
Cfd	CGTACCATGACGGGGTAGTC	ATCCGGTAGGATGACTCG
Col1a1	GTGCTCCTGGTATTGCTGGT	GGCTCCTCGTTTTCTTCTT
Col1a2	GCCACCATTGATAGTCTCTCC	CACCCAGCGAAGAACTCATA
Col3a1	GGGTTTCCCTGGTCCTAAAG	CCTGGTTTCCCATTTTCTCC
Fasn	TTGCTGGCACTACAGAATGC	AACAGCCTCAGAGCGACAAT
Fgf21	CTGCTGGGGTCTACCAAG	CTGCGCTACCACTGTTCC
Hnf1a	GACCTGACCGAGTTGCCTAAT	CCGGCTCTTTCAGAATGGGT
Il1b	CTGGTGTGTGACGTTCCCATTA	CCGACAGCACGAGGCTTT
Il6	ACAACCACGGCCTTCCCTACTT	CACGATTTCCAGAGAACATGTG
Pepck1	TCATCATCACCCAAGAGCAG	CACATAGGGCGAGTCTGTCA
Rps18	CATGCAGAACCCACGACAGTA	CCTCACGCAGCTTGTTGTCTA
Scd1	CGCCCAAGCTGGAGTACGTC	CGCCCAAGCTGGAGTACGTC
Srebp1c	CTGGCAGTTCCATTGACAAG	ACTGAAGCTGGTGACTGCTG
Tgfb1	TGCGCTTGCAGAGATTA AAA	AGCCCTGTATTCCGTCTCCT
Tlr4	TGTCATCAGGGACTTTGCTG	GGACTCTGATCATGGCACTG
Tnfa	ACGGCATGGATCTCAAAGAC	AGATAGCAAATCGGCTGACG
Trem2	CTACCAGTGTCAGAGTCTCCGA	CCTCGAAACTCGATGACTCCTC

379 **References**

- 380 1 Ge, X., Zheng, L., Wang, M., Du, Y. & Jiang, J. Prevalence trends in non-alcoholic fatty  
381 liver disease at the global, regional and national levels, 1990-2017: a population-based  
382 observational study. *BMJ Open* **10**, e036663 (2020). [https://doi.org/10.1136/bmjopen-](https://doi.org/10.1136/bmjopen-2019-036663)  
383 [2019-036663](https://doi.org/10.1136/bmjopen-2019-036663)
- 384 2 Younossi, Z. *et al.* Global burden of NAFLD and NASH: trends, predictions, risk factors  
385 and prevention. *Nat Rev Gastroenterol Hepatol* **15**, 11-20 (2018).  
386 <https://doi.org/10.1038/nrgastro.2017.109>
- 387 3 Ferguson, D. & Finck, B. N. Emerging therapeutic approaches for the treatment of  
388 NAFLD and type 2 diabetes mellitus. *Nat Rev Endocrinol* **17**, 484-495 (2021).  
389 <https://doi.org/10.1038/s41574-021-00507-z>
- 390 4 Friedman, S. L., Neuschwander-Tetri, B. A., Rinella, M. & Sanyal, A. J. Mechanisms of  
391 NAFLD development and therapeutic strategies. *Nat Med* **24**, 908-922 (2018).  
392 <https://doi.org/10.1038/s41591-018-0104-9>
- 393 5 Stefan, N., Haring, H. U. & Cusi, K. Non-alcoholic fatty liver disease: causes, diagnosis,  
394 cardiometabolic consequences, and treatment strategies. *Lancet Diabetes Endocrinol* **7**,  
395 313-324 (2019). [https://doi.org/10.1016/S2213-8587\(18\)30154-2](https://doi.org/10.1016/S2213-8587(18)30154-2)
- 396 6 Kim, H. *et al.* Metabolic Spectrum of Liver Failure in Type 2 Diabetes and Obesity: From  
397 NAFLD to NASH to HCC. *Int J Mol Sci* **22** (2021). <https://doi.org/10.3390/ijms22094495>
- 398 7 Duell, P. B. *et al.* Nonalcoholic Fatty Liver Disease and Cardiovascular Risk: A Scientific  
399 Statement From the American Heart Association. *Arterioscler Thromb Vasc Biol* **42**,  
400 e168-e185 (2022). <https://doi.org/10.1161/ATV.000000000000153>
- 401 8 Kasper, P. *et al.* NAFLD and cardiovascular diseases: a clinical review. *Clin Res Cardiol*  
402 **110**, 921-937 (2021). <https://doi.org/10.1007/s00392-020-01709-7>
- 403 9 Barreby, E., Chen, P. & Aouadi, M. Macrophage functional diversity in NAFLD - more  
404 than inflammation. *Nat Rev Endocrinol* **18**, 461-472 (2022).  
405 <https://doi.org/10.1038/s41574-022-00675-6>
- 406 10 Cai, J., Zhang, X. J. & Li, H. The Role of Innate Immune Cells in Nonalcoholic  
407 Steatohepatitis. *Hepatology* **70**, 1026-1037 (2019). <https://doi.org/10.1002/hep.30506>
- 408 11 Guilliams, M. & Scott, C. L. Liver macrophages in health and disease. *Immunity* **55**,  
409 1515-1529 (2022). <https://doi.org/10.1016/j.immuni.2022.08.002>
- 410 12 Park, S. J., Garcia Diaz, J., Um, E. & Hahn, Y. S. Major roles of kupffer cells and  
411 macrophages in NAFLD development. *Front Endocrinol (Lausanne)* **14**, 1150118 (2023).  
412 <https://doi.org/10.3389/fendo.2023.1150118>
- 413 13 Sakai, M. *et al.* Liver-Derived Signals Sequentially Reprogram Myeloid Enhancers to  
414 Initiate and Maintain Kupffer Cell Identity. *Immunity* **51**, 655-670 e658 (2019).  
415 <https://doi.org/10.1016/j.immuni.2019.09.002>
- 416 14 Krenkel, O. *et al.* Myeloid cells in liver and bone marrow acquire a functionally distinct  
417 inflammatory phenotype during obesity-related steatohepatitis. *Gut* **69**, 551-563 (2020).  
418 <https://doi.org/10.1136/gutjnl-2019-318382>
- 419 15 Guilliams, M. *et al.* Spatial proteogenomics reveals distinct and evolutionarily conserved  
420 hepatic macrophage niches. *Cell* **185**, 379-396 e338 (2022).  
421 <https://doi.org/10.1016/j.cell.2021.12.018>
- 422 16 Govaere, O. *et al.* Transcriptomic profiling across the nonalcoholic fatty liver disease  
423 spectrum reveals gene signatures for steatohepatitis and fibrosis. *Sci Transl Med* **12**  
424 (2020). <https://doi.org/10.1126/scitranslmed.aba4448>
- 425 17 Merle, N. S., Church, S. E., Fremeaux-Bacchi, V. & Roumenina, L. T. Complement  
426 System Part I - Molecular Mechanisms of Activation and Regulation. *Front Immunol* **6**,  
427 262 (2015). <https://doi.org/10.3389/fimmu.2015.00262>

- 428 18 Kolev, M. & Kemper, C. Keeping It All Going-Complement Meets Metabolism. *Front Immunol* **8**, 1 (2017). <https://doi.org/10.3389/fimmu.2017.00001>
- 429
- 430 19 Zhao, J. *et al.* Association of complement components with the risk and severity of
- 431 NAFLD: A systematic review and meta-analysis. *Front Immunol* **13**, 1054159 (2022).
- 432 <https://doi.org/10.3389/fimmu.2022.1054159>
- 433 20 Segers, F. M. *et al.* Complement alternative pathway activation in human nonalcoholic
- 434 steatohepatitis. *PLoS One* **9**, e110053 (2014).
- 435 <https://doi.org/10.1371/journal.pone.0110053>
- 436 21 Markiewski, M. M. & Lambris, J. D. The role of complement in inflammatory diseases
- 437 from behind the scenes into the spotlight. *Am J Pathol* **171**, 715-727 (2007).
- 438 <https://doi.org/10.2353/ajpath.2007.070166>
- 439 22 Yadav, M. K. *et al.* Molecular basis of anaphylatoxin binding, activation, and signaling
- 440 bias at complement receptors. *Cell* **186**, 4956-4973 e4921 (2023).
- 441 <https://doi.org/10.1016/j.cell.2023.09.020>
- 442 23 Flier, J. S., Cook, K. S., Usher, P. & Spiegelman, B. M. Severely impaired adiponin
- 443 expression in genetic and acquired obesity. *Science* **237**, 405-408 (1987).
- 444 <https://doi.org/10.1126/science.3299706>
- 445 24 Xu, Y. *et al.* Complement activation in factor D-deficient mice. *Proc Natl Acad Sci U S A*
- 446 **98**, 14577-14582 (2001). <https://doi.org/10.1073/pnas.261428398>
- 447 25 Lim, J. *et al.* C5aR and C3aR antagonists each inhibit diet-induced obesity, metabolic
- 448 dysfunction, and adipocyte and macrophage signaling. *FASEB J* **27**, 822-831 (2013).
- 449 <https://doi.org/10.1096/fj.12-220582>
- 450 26 Polyzos, S. A., Kountouras, J. & Mantzoros, C. S. Adipokines in nonalcoholic fatty liver
- 451 disease. *Metabolism* **65**, 1062-1079 (2016).
- 452 <https://doi.org/10.1016/j.metabol.2015.11.006>
- 453 27 Han, J. & Zhang, X. Complement Component C3: A Novel Biomarker Participating in the
- 454 Pathogenesis of Non-alcoholic Fatty Liver Disease. *Front Med (Lausanne)* **8**, 653293
- 455 (2021). <https://doi.org/10.3389/fmed.2021.653293>
- 456 28 Lo, J. C. *et al.* Adiponin is an adipokine that improves beta cell function in diabetes. *Cell*
- 457 **158**, 41-53 (2014). <https://doi.org/10.1016/j.cell.2014.06.005>
- 458 29 Gomez-Banoy, N. *et al.* Adiponin preserves beta cells in diabetic mice and associates with
- 459 protection from type 2 diabetes in humans. *Nat Med* **25**, 1739-1747 (2019).
- 460 <https://doi.org/10.1038/s41591-019-0610-4>
- 461 30 Mamane, Y. *et al.* The C3a anaphylatoxin receptor is a key mediator of insulin resistance
- 462 and functions by modulating adipose tissue macrophage infiltration and activation.
- 463 *Diabetes* **58**, 2006-2017 (2009). <https://doi.org/10.2337/db09-0323>
- 464 31 Han, J. *et al.* Bone marrow-derived macrophage contributes to fibrosing steatohepatitis
- 465 through activating hepatic stellate cells. *J Pathol* **248**, 488-500 (2019).
- 466 <https://doi.org/10.1002/path.5275>
- 467 32 Boland, M. L. *et al.* Towards a standard diet-induced and biopsy-confirmed mouse model
- 468 of non-alcoholic steatohepatitis: Impact of dietary fat source. *World J Gastroenterol* **25**,
- 469 4904-4920 (2019). <https://doi.org/10.3748/wjg.v25.i33.4904>
- 470 33 Hansen, H. H. *et al.* Human translatability of the GAN diet-induced obese mouse model
- 471 of non-alcoholic steatohepatitis. *BMC Gastroenterol* **20**, 210 (2020).
- 472 <https://doi.org/10.1186/s12876-020-01356-2>
- 473 34 Vacca, M. *et al.* An unbiased ranking of murine dietary models based on their proximity
- 474 to human metabolic dysfunction-associated steatotic liver disease (MASLD). *Nat Metab*
- 475 (2024). <https://doi.org/10.1038/s42255-024-01043-6>
- 476 35 Uhlen, M. *et al.* Proteomics. Tissue-based map of the human proteome. *Science* **347**,
- 477 1260419 (2015). <https://doi.org/10.1126/science.1260419>

- 478 36 MacParland, S. A. *et al.* Single cell RNA sequencing of human liver reveals distinct  
479 intrahepatic macrophage populations. *Nat Commun* **9**, 4383 (2018).  
480 [https://doi.org:10.1038/s41467-018-06318-7](https://doi.org/10.1038/s41467-018-06318-7)
- 481 37 Tabula Muris, C. *et al.* Single-cell transcriptomics of 20 mouse organs creates a Tabula  
482 Muris. *Nature* **562**, 367-372 (2018). [https://doi.org:10.1038/s41586-018-0590-4](https://doi.org/10.1038/s41586-018-0590-4)
- 483 38 Suppli, M. P. *et al.* Hepatic transcriptome signatures in patients with varying degrees of  
484 nonalcoholic fatty liver disease compared with healthy normal-weight individuals. *Am J*  
485 *Physiol Gastrointest Liver Physiol* **316**, G462-G472 (2019).  
486 [https://doi.org:10.1152/ajpgi.00358.2018](https://doi.org/10.1152/ajpgi.00358.2018)
- 487 39 Ma, L. *et al.* Adipsin and Adipocyte-derived C3aR1 Regulate Thermogenic Fat in a Sex-  
488 dependent Fashion. *JCI Insight* (2024). [https://doi.org:10.1172/jci.insight.178925](https://doi.org/10.1172/jci.insight.178925)
- 489 40 Kong, L. R. *et al.* Loss of C3a and C5a receptors promotes adipocyte browning and  
490 attenuates diet-induced obesity via activating inosine/A2aR pathway. *Cell Rep* **42**,  
491 112078 (2023). [https://doi.org:10.1016/j.celrep.2023.112078](https://doi.org/10.1016/j.celrep.2023.112078)
- 492 41 Li, X. *et al.* A new NASH model in aged mice with rapid progression of steatohepatitis  
493 and fibrosis. *PLoS One* **18**, e0286257 (2023).  
494 [https://doi.org:10.1371/journal.pone.0286257](https://doi.org/10.1371/journal.pone.0286257)
- 495 42 Cumpelik, A. *et al.* Dynamic regulation of B cell complement signaling is integral to  
496 germinal center responses. *Nat Immunol* **22**, 757-768 (2021).  
497 [https://doi.org:10.1038/s41590-021-00926-0](https://doi.org/10.1038/s41590-021-00926-0)
- 498 43 Zhang, X., Goncalves, R. & Mosser, D. M. The isolation and characterization of murine  
499 macrophages. *Curr Protoc Immunol* **Chapter 14**, 14 11 11-14 11 14 (2008).  
500 [https://doi.org:10.1002/0471142735.im1401s83](https://doi.org/10.1002/0471142735.im1401s83)  
501